Comparing field, probabilistic, and 2D numerical approaches to assess gravel mobility in a gravel-bed river

Fanny Arnaud, André Paquier, Daniel Vazquez-tarrio, B. Camenen, Jérôme Le Coz, Kristell Michel, G Naudet, Hervé Pella, Hervé Piégay

Check for updates

ADVANCING EARTH AND SPACE SCIENCES

Water Resources Research

RESEARCH ARTICLE
10.1029/2022WR034127

Key Points:
- PIT-tagged gravels are used to track gravel mobility in the restored Ain River
- The results of field tracer surveys are compared with probabilistic and two-dimensional numerical modeling
- The three approaches are found to be meaningful and complementary

Correspondence to:
F. Arnaud,
fanny.arnaud@ens-lyon.fr

Citation:
Arnaud, F., Paquier, A., Vázquez-Tarrío, D., Camenen, B., Le Coz, J., Michel, K., et al. (2023). Comparing field, probabilistic, and 2D numerical approaches to assess gravel mobility in a gravel-bed river. *Water Resources Research*, *59*, e2022WR034127. https://doi.org/10.1029/2022WR034127

Received 15 NOV 2022
Accepted 8 SEP 2023

Author Contributions:
Conceptualization: F. Arnaud, A. Paquier, D. Vázquez-Tarrío, B. Camenen, J. Le Coz, H. Piégay
Data curation: F. Arnaud, A. Paquier
Formal analysis: F. Arnaud, A. Paquier, D. Vázquez-Tarrío, B. Camenen, J. Le Coz, K. Michel, G. Naudet
Funding acquisition: H. Piégay
Investigation: F. Arnaud, A. Paquier, D. Vázquez-Tarrío, K. Michel, G. Naudet
Methodology: F. Arnaud, A. Paquier, D. Vázquez-Tarrío, K. Michel, G. Naudet, H. Pella, H. Piégay
Project Administration: H. Piégay
Resources: A. Paquier, K. Michel, H. Pella
Software: A. Paquier, B. Camenen, J. Le Coz, G. Naudet, H. Pella
Supervision: F. Arnaud, H. Piégay
Validation: A. Paquier, B. Camenen, J. Le Coz, H. Piégay
Writing – original draft: F. Arnaud, A. Paquier, D. Vázquez-Tarrío, J. Le Coz

Comparing Field, Probabilistic, and 2D Numerical Approaches to Assess Gravel Mobility in a Gravel-Bed River

F. Arnaud[1,2], A. Paquier[2,3], D. Vázquez-Tarrío[4], B. Camenen[2,3], J. Le Coz[2,3], K. Michel[1,2], G. Naudet[2,3], H. Pella[2,3], and H. Piégay[1,2]

[1]UMR 5600 EVS, CNRS/University of Lyon/ENS de Lyon, Lyon Cedex 07, France, [2]LTSER, CNRS/Zone Atelier Bassin du Rhône/GRAIE, Villeurbanne, France, [3]INRAE, UR RiverLy, Villeurbanne, France, [4]Universidad Complutense de Madrid/Departamento de Geodinámica, Estratigrafía y Paleontología/C. de José Antonio Novais, Madrid, Spain

Abstract Sediment transport is a key process that affects the morphology and ecological habitat diversity of rivers. As part of a gravel augmentation program to mitigate sediment deficit below a dam, gravel mobility in the Ain River in Eastern France was investigated by tracking of a large amount (n = 1,063) of PIT-tagged gravels in the field, conducting a probabilistic approach based on published tracer studies, and performing two-dimensional (2D) numerical modeling of flow and bedload transport. This comparative study highlights the strengths, weaknesses, and complementary aspects of the three approaches to the understanding of river gravel mobility. Thanks to recent technological improvements, PIT-tagged gravels provide an increasingly reliable and accurate representation of bedload movement in the field, although it remains limited in spatio-temporal resolution. Based on an exponential distribution, the probabilistic approach correctly reproduces the average trend in travel distances by the different classes of particles over hydrological periods, including one or several significant floods. Furthermore, the 2D numerical modeling accounts for the variability of local hydrodynamic conditions and can simulate realistic displacement distributions for the different classes of particles with high spatio-temporal resolution. Numerical modeling is a very encouraging approach, which makes our study original because it is the first time that the estimation of mean travel distances, the application of an exponential distribution, and the comparison with a hydrodynamic model are combined. A more effective modeling strategy involves incorporating a probabilistic transport model in the 2D numerical model to reproduce the observed scatter of the individual particle trajectories.

1. Introduction

Sediment transport is a key process that affects the morphology and ecological habitat diversity of rivers. Understanding bed mobility is necessary to assess the impacts of human disturbances (e.g., damming, gravel mining, embankments) on river morphodynamics and to help design efficient management and restoration measures (Grabowski et al., 2014; Piégay et al., 2016b). Sediment augmentation, that is, the artificial addition of sediments into the channel, is increasingly used to mitigate sediment deficit impacts below dams (Kondolf et al., 2014). Additionally, field monitoring is required to assess the efficiency of the restoration measure, by providing key information on the kinematics of sediment wave propagation in the restored reach, morphological evolutions or bed grain size changes (Arnaud et al., 2017; Vázquez-Tarrío et al., 2023). Field-measured data can also feed morphodynamic models, which can be developed to accurately evaluate and predict sediment mobility and assess channel evolution scenarios.

Fluvial geomorphologists have long used tagged gravels to measure the bedload mobility of gravel-bed rivers (e.g., Keller, 1970; Laronne & Carson, 1976). The main interests of tracking the displacement of individual particles are to understand initial motion criteria for gravel, size-selective transport processes, morphological controls on gravel dispersion, and spatial patterns of bedload transport when coupled with detailed morphological surveys (Vericat et al., 2017). In the early 2000s, radio-frequency identification (RFID) technology with low-frequency passive integrated transponder (PIT) tags opened new opportunities because of their low cost (<€5 per tag), long operating life (>10 years, as they contain no battery), small tag size, and unique identification codes permitting to locate buried or exposed particles (Arnaud et al., 2015; Chapuis et al., 2014). However, the first studies using PIT-tagged gravels were restricted to small, shallow streams (channel width <25 m) because of the decimetric detection range and the extensive fieldwork needed to obtain sufficient recovery rates (Bradley & Tucker, 2012; Lamarre et al., 2005; Schneider et al., 2010). Developments of RFID devices, such as larger antennas (up to

Writing – review & editing: F. Arnaud, A. Paquier, D. Vázquez-Tarrío, B. Camenen, J. Le Coz, H. Piégay

2 m long) that cover larger search areas, and the development of procedures using a boat to detect tracers in deeper water and conditions with fairly high flow velocity have improved the performance of the tracer method (Arnaud et al., 2015). With the enhanced procedures, PIT tags have been successfully used for monitoring gravel augmentation in the 100 m-wide regulated channel of the Rhine River (Arnaud et al., 2017; Chardon et al., 2021). However, PIT-tag studies are often challenged by limited recovery rates, especially in highly-dynamic rivers (Camenen et al., 2010), which makes tracer data a questionable representation of the bedload movement in the field. Loss of tracer particles can be due to the non-recovery of buried tracers, signal interference when tags are too close to each other, incomplete prospection of the surveyed area, or tracers traveling further than the prospected area (Cassel et al., 2020). A critical analysis of the methods is therefore required before interpreting the mobility of gravel-bed rivers from field tracer data.

A number of meta-analysis of tracer data sets have been produced in many gravel- and coarse-bed rivers. This corpus is useful to contextualize and analyze the data from new tracer experiments (Hassan & Bradley, 2017; Vázquez-Tarrío & Batalla, 2019; Vázquez-Tarrío et al., 2019). In addition, previous studies have tried to predict the distribution of particle displacements for a given site and streamflow, especially because survey costs for repeated sediment tracking can be high (Cassel et al., 2020). For a given type of channel morphology, statistically significant correlations between mean tracer travel distances and dimensionless peak stream power can be found, as reported by Vázquez-Tarrío et al. (2019) in a review of tracer data. The distribution of particle travel distances has typically been approximated with exponential or gamma probability distribution functions, which seem to fit the available field observations reasonably well (Bradley, 2017; Clark et al., 2022; Hassan & Bradley, 2017; Liébault et al., 2012; Phillips & Jerolmack, 2014).

Alongside the exploitation of field tracer data, numerical modeling of the flow dynamics can assist the decision-making in river restoration projects, especially to choose between different designs of gravel augmentation (El Kadi Abderrezzak et al., 2016; Juez et al., 2016; Stähly et al., 2020). To date, some studies have compared field tracer data and numerical modeling outcomes (Biron et al., 2012; Chapuis et al., 2015; Liedermann et al., 2013; Milan, 2013; Roberts et al., 2020). Two-dimensional (2D) numerical modeling is generally based on the resolution of the Barré-de-Saint-Venant equations, along with the Exner equation and semi-empirical formulations of bedload (Amoudry & Souza, 2011; Williams et al., 2016). Such models can predict sediment transport, bed elevation changes, and erosional and depositional patterns along the river channel over time. The modeling performance was assessed using laboratory experiments (El Kadi Abderrezzak et al., 2016; Juez et al., 2016) or using field experiments for rivers with poorly sorted sediments (Gaeuman, 2014). Numerical modeling can help understand the physical parameters that regulate particle displacements by estimating the spatial distribution of bed shear stresses, bedload transport capacity, and flow and bedload directions at peak flow (Chapuis et al., 2015) or different flow stages (Biron et al., 2012; Liedermann et al., 2013; Milan, 2013; Roberts et al., 2020). Numerical modeling provides results with a high spatio-temporal resolution but often with large uncertainties, mainly due to the lack of data for the calibration of sediment transport processes. In addition, 2D modeling is based on Eulerian perspective and it does not provide direct Lagrangian results such as the information provided by tracer data (Amoudry & Souza, 2011; Williams et al., 2016). Hence, more field-measured data are required to calibrate and validate numerical models and assess the performance of sediment transport equations used in classical 2D modeling.

Therefore, this paper aims to analyze coarse sediment displacement by testing three approaches: (a) field observations of PIT-tagged gravels, (b) a probabilistic approach based on previous data compiled from the literature to assess field data quality; and (c) 2D numerical modeling, to relate particle path characteristics with flow hydraulics. To our knowledge, this study is the first to use such a high number of PIT tags ($n = 1{,}063$) in a medium-sized meandering gravel-bed river (90 m wide), and to compare field observations with expected travel distances inferred from previous literature using a probabilistic approach and with results from 2D hydrodynamic modeling to evaluate and discuss data accuracy. We investigate gravel mobility in the Ain River in Eastern France in the context of a gravel augmentation program to mitigate sediment deficit below a dam.

2. Study Site

2.1. The Lower Ain River

The Ain River in Eastern France drains a watershed of 3,630 km^2, starting from the Jura Mountains. The 50 km-long lower river segment extends from the Allement Dam to the confluence with the Rhône River (Figure 1a). The Ain River is among the few remaining tributaries that supply significant amounts of coarse

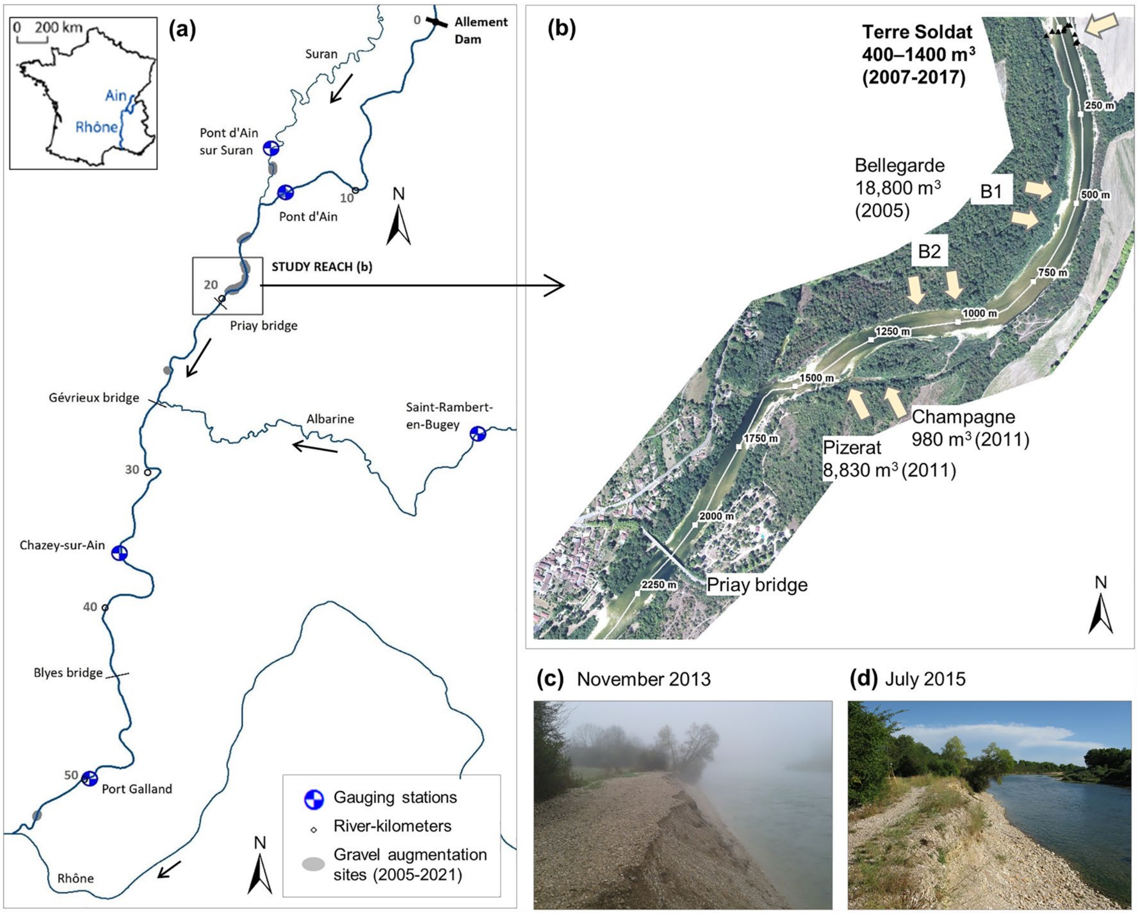

Figure 1. (a) Map of the Lower Ain River. (b) Aerial view of the Terre Soldat/Priay site (Base map: ORTHO HR® IGN 2015). Gravel augmentation operations conducted since 2005 are indicated by arrows. Markers are indicated every 250 m on the channel centerline. The positions of seeded tracers are indicated with black triangles. (c) Photo of the left bank at Terre Soldat in November 2013, just after the supply of 1,300 m^3 of gravel, and (d) in July 2015, after flood events that remobilized the gravel supply.

sediments to the Rhône River. The mean annual discharge of the Lower Ain, recorded at the Chazey-sur-Ain gauging station downstream of our study site (Figure 1a) over the 1959–2017 period, is 120 m^3/s, and the 2-, 10-, and 50-year floods are ∼760, 1,150, and 1,500 m^3/s, respectively. The low-flow discharge is 16 m^3/s (information from the national discharge database, http://www.hydro.eaufrance.fr). The channel is 90 m wide on average and the mean slope is 0.0011 m/m (Rollet, 2007).

Compared with other European rivers of this size, the Lower Ain remains unusually close to its natural state since it still features freely developing shifting meanders. It has been unaffected by in-channel gravel mining and very few embankments are found along its course (Muhar et al., 2019). However, its morphodynamics have been disturbed by a cascade of dams built on its upper course. Below the last dam (Allement Dam, built in 1960), the Lower Ain is affected by a sediment deficit of 15,000 m^3/yr, with a bed armoring front ($D_{50} \sim 80$ mm) prograding downstream at a celerity of approximately 500 m/yr (Rollet, 2007; Rollet et al., 2014). Bed incision has lowered the water level by approximately 1 m since the 1950s. This degradation caused several abandoned channels to dry out and the original riparian communities have been replaced by more terrestrial species (Marston et al., 1995). The reach downstream of Priay is still actively shifting and creating cut-off channels. In the 2000s, restoration measures combined the excavation and reconnection of cut-off channels, and in-channel gravel augmentation in the upstream reach, to maintain bedload transport downstream and preserve the free-meandering pattern. Between 2005 and 2021, seven cut-off channels have been rehabilitated, and 95,000 m^3 of gravel have been supplied to the main channel by the Lower Ain River syndicate (SR3A). The gravel was extracted from the restored channels and the lowest tributary, the Albarine River, because its sediment transport is regularly interrupted by a narrow bridge near its confluence with the Ain River (see locations in Figures 1a and 1b).

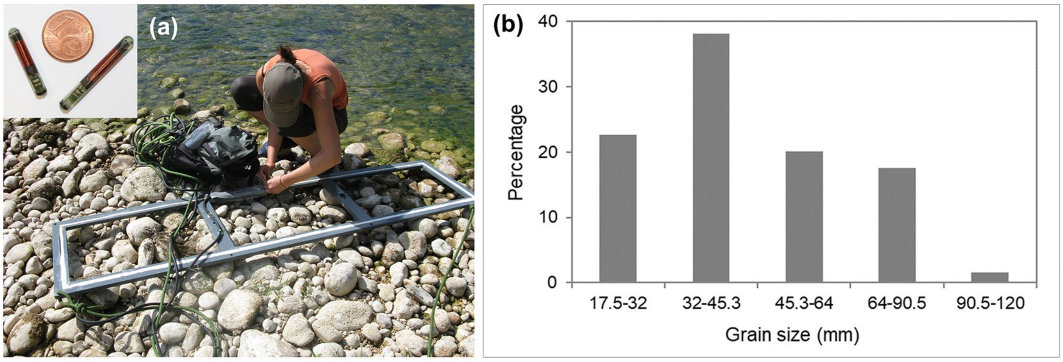

Figure 2. (a) 23 mm- and 32 mm-long passive integrated transponder tags and the 2 m-long detection antenna used in this study. (b) Grain size distribution of the PIT-tagged particles.

2.2. The Terre Soldat/Priay Reach

The study site is located on the sediment-starved reach of the Lower Ain River, between the Terre Soldat bank and the downstream part of the Priay village (Figure 1b). The discharge that is representative of this reach corresponds to the addition of discharges measured in the Ain River and the Suran River (right-bank tributary, mean annual discharge of 6 m^3/s) at Pont d'Ain gauging stations (Figure 1a).

The Terre Soldat/Priay reach is a useful site for studying bedload mobility on a sediment-starved, armored riverbed where gravel augmentation has been conducted. The 4 km-long reach is a pool-riffle series with discontinuous limestone outcrops and a few small gravel bars. Priay was the location reached by the downstream front of the sediment deficit in the 2010s (Rollet et al., 2014). The 950 m-long left bank at Terre Soldat is the only bank along this reach with active erosion, as seen in comparing aerial photographs from 1971 to 2008. Since 2007, the upstream section of the bank has been supplied almost annually with 400–1,400 m^3 of sediment originating from channel dredging in the vicinity of a bridge in the Albarine tributary (Figures 1c and 1d). The injected sediment was deposited on the bank without sorting or compaction. Surface Wolman pebble counts made on the dredging site showed a D_{50} and D_{84} of 22 and 39 mm, respectively.

3. Materials and Methods

Bedload tracking using PIT tags was best suited for monitoring gravel augmentation in the Ain River than other methods, such as repeated topographic surveys, because the introduced volume of sediment was modest (1,300 m^3) and propagated downstream over a long reach. The detection of the sediment wave through conventional topography with decimetric vertical uncertainty would have been challenging. Thus, we focused on particle tracking. Data sets for this research (particle tracking, probabilistic and numerical modeling results) are freely available in the PANGAEA data repository (Arnaud et al., 2023).

3.1. Particle Tracking

3.1.1. Field Surveys

The RFID equipment used in this study was previously described by Arnaud et al. (2015). It is composed of a reader system connected to a small (0.5 m diameter), medium (0.4 × 1.1 m), or large (0.4 × 2.0 m) detection antenna that is held by an operator over gravel bars and in shallow waters, or towed by a boat in waters deeper than 0.6 m. Tags, readers and the small antenna were manufactured by Texas Instruments and commercialized by the company CIPAM (France). The medium and large antennas were home-made (see Arnaud et al., 2015). We equipped 1,063 particles with PIT tags. We used mostly 32 mm-long tags ($n = 896$) because the reading range is up to 50% higher than 23 mm-long tags (Arnaud et al., 2015) (Figure 2a), but 23 mm-long tags were also used to equip smaller particles. The median grain size of the PIT-tagged gravels was 41 mm and the minimum diameter was 18 mm (Figure 2b). We drilled pebbles along the *c*-axis to maximize the probability of recovering vertical tags based on the preferential arrangement of particles on the riverbed (Arnaud et al., 2015).

We released tracer particles on 18 November 2013, a few weeks after the Terre Soldat bank was supplied with 1,300 m^3 of fresh gravel (Figure 1c). We deposited 10 patches of one hundred particles onto the bank and the

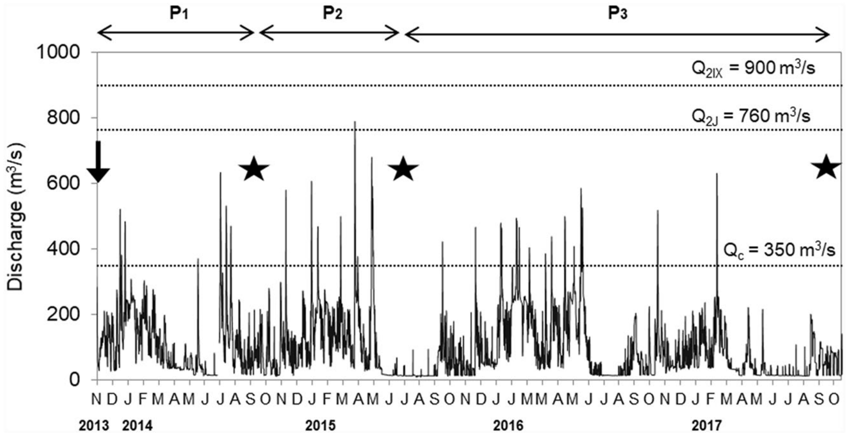

Figure 3. Discharge time series averaged over 2 hours at Pont d'Ain + Suran gauging stations from 2013 to 2017. The arrow and the stars indicate the dates of tracer release and tracking surveys. Q_c: critical discharge for the incipient bedload. Q_{2J}: 2-year daily discharge. Q_{2IX}: 2-year instantaneous discharge.

riverbed: three patches on the bank top, two patches on the bank bottom, and five patches deployed from a boat along a cross-section in the adjacent channel. Tracer patches were placed without specific imbrication into the bed structure. The grain size distribution in each patch was similar to the distribution of the whole tracer sample. Tracer positions were tracked in September 2014, July 2015, and September–October 2017, noted as surveys S_i, which define three hydrological periods P_i (Figure 3). From November 2013 to September 2014 (P_1), six flood events yielded discharges higher than the critical discharge for the incipient bedload (Q_c estimated at 350 m^3/s from painted plots made on gravel bars along the Lower Ain River; Rollet, 2007), with a maximum discharge $Q_{\max}$ at 630 m^3/s. From September 2014 to July 2015 (P_2), six flood events occurred, including a flood that exceeded the 2-year flood daily discharge ($Q_{\max} = 790$ m^3/s). For logistic reasons, the tracking survey was not conducted in 2016, thus the period P_3 lasted more than 2 years and covered 12 flood events that were higher than Q_c ($Q_{\max} = 630$ m^3/s).

During the wading surveys, the tracer positions and IDs were manually recorded using a GPS (Trimble GeoXH or GeoXT, XYZ accuracy <0.5 m). During the 2015 boat surveys, a differential GPS (DGPS Trimble 5800 RTK, XYZ accuracy <0.05 m) was used. The method was improved in 2017 by connecting the RFID reader to a tablet computer and a GPS (Geomax Zenith 35, XYZ accuracy <0.05 m), which automatically recorded the tracer positions and IDs (NMEA track; ArpenGIS software). It suppressed errors in writing the tracer IDs and delays between the tracer detection beep signal and the manual DGPS logging, especially in areas where several tracers were detected in a short time. The boat surveys were performed longitudinally to keep the position of the antenna relatively fixed with respect to the onboard GPS and to allow for post-processing of XY tracer coordinates by subtracting the distance from the antenna. The tracking area increased as the gravel propagated downstream, from an 870 m-long reach covering 4.1 ha (2014 tracking) to a 3.9 km-long reach covering 16.7 ha (2017 tracking). The GPS course was systematically recorded to identify areas that were already searched. The 2015 and 2017 surveys correspond to 71.2 and 79.3 km in total lengths of GPS courses, respectively. The 2014 survey was only partially performed and the GPS course was not recorded.

3.1.2. Tracer Recovery Rates and Data Accuracy

The 2014 partial tracking survey was performed by two operators for 1.5 days only. Nevertheless, it allowed us to detect 329 tracers (including double reading positions). The 2015 survey required two to four operators over 5.5 days, which allowed the detection of 825 tracers (also including multiple positions). The 2017 survey took the same time with two operators, and 617 tracers were detected (including multiple positions).

Notably, a tracer can be detected by boat and wading searches several times within the same survey. We compared the position of each multiple detection of the same tracer to evaluate tracer geolocation accuracy (2014: $n = 64$ doubles, triplets, etc.; 2015: $n = 317$; 2017: $n = 238$). For example, in 2017, 60% of the double reading positions were separated by less than 5 m, and 16% were separated by 5–10 m. We retained ±10 m for horizontal accuracy, including the potential movement of the antenna (which was not placed at a systematically fixed distance from the boat) and GPS accuracy. One of the double reading positions was retained. The remaining 24% of the double reading positions were separated by 15 m on average. All of these corresponded to tracers detected in the boat

10.1029/2022WR034127

ascent and descent. Therefore, the middle position between the double readings was also retained. For the 2014 and 2015 tracking surveys, we corrected most of the double tracer positions separated by more than 10 m by examining the previous positions and displacement trajectories. Double tracer positions that were substantially separated by over 10 m or exhibited aberrant trajectories were mainly observed due to the use of the GPS GeoXH on the boat, which required several seconds of delay between the detection beep signal and the manual ID logging. This required us to exclude 31 tracers from the statistical analysis for the 2014 survey.

Following MacVicar and Papangelakis (2022), we added inferred tracers to the tracer population in S_i, that is, tracers missing in S_i that were found in both S_{i-1} (or S_{i-2}) and S_{i+1} and remained immobile throughout. This substantially increased the number of tracers in the 2014 partial survey (+92 inferred tracers) and 2015 survey (+18 inferred tracers).

Moreover, since the tracers from patches number 4 and 5 seeded near the right bank remained on site (Figure 5a), we removed these two patches from the travel distance and trajectory analysis. Thus, the statistical analysis was based on 862 seeded tracers instead of 1,063. The number of recovered (including inferred) tracers was 321, 473, and 344 particles in the three successive surveys, respectively. This corresponds to recovery rates of 37%, 55%, and 40%, respectively.

3.1.3. Data Analysis

We measured the distances traveled by tracers by projecting the tracer positions onto the channel centerline using the linear referencing tool in ArcMap version 10.8 (ESRI). We calculated two classical metrics based on the individual tracers found in successive surveys: the travel distance between surveys S_{i-1} and S_i, and the cumulated travel distance from the initial seeding position (S_0). The travel distance L_T (in m) of the tracer cloud centroid was also defined as:

$$L_T = C_{T,\mathrm{Si}} - C_{T,\mathrm{Si-1}} \tag{1}$$

where $C_{T,\mathrm{Si}} = \sum_{t=1}^{n_{\mathrm{stat}}} x_{t,\mathrm{Si}} / n_{\mathrm{stat}}$ is the longitudinal tracer cloud centroid (average) position on the channel centerline in survey S_i, and $x_{t,\mathrm{Si}}$ is the longitudinal tracer position in survey S_i (Arnaud et al., 2017).

The tracer cloud centroid metric uses all the tracer positions that were observed and inferred in a given survey, assuming that the tracer cloud is representative of the whole tracer sample (Haschenburger, 2013). On the Rhine River, Arnaud et al. (2017) recommended using the tracer cloud centroid because this metric is easily measurable and it informs on the timeframe of sediment wave propagation. In addition, the kinematics of sediment pulse can be specified with the virtual velocity, which is the average tracer velocity over the transporting event including periods of rest and motion (Hassan et al., 1992). The virtual velocity (in m/h) for each period P_i was calculated as:

$$V_{\mathrm{Pi}} = \frac{\overline{L_{\mathrm{sm}}}}{t_{Q_c}} \tag{2}$$

where $\overline{L_{\mathrm{sm}}}$ is the mean travel distance (in meters) based on individual and same, mobile tracers that were recovered in surveys S_{i-1} and S_i, and t_{Q_c} is the time (in hours) during which the discharge was greater than Q_c. We used the discharge time series (averaged over 2 hours) based on the sum of values at Pont d'Ain and Suran gauging stations.

Finally, the grain size effect on tracer displacement was analyzed by dividing the tracer cloud of each survey into five separate tracer clouds corresponding to one of the particle size classes described in Figure 2b.

3.2. Probabilistic Approach

Vázquez-Tarrío et al. (2019) reported a statistically significant correlation between the dimensionless (peak) stream power and the mean travel distance of particles, using a large data set of tracer studies compiled from the literature. In their analysis, the mean travel distance $\overline{L}$ was normalized by the "morphological length" of the channel (i.e., average step-pool and riffle-pool spacing), and they computed the dimensionless peak unit stream power ω^* based on Eaton and Church (2011):

$$\omega^* = \frac{\omega}{\rho \cdot (g \cdot R_g \cdot D_{50})^{\frac{3}{2}}} \tag{3}$$

where $\omega = \frac{\rho \cdot g \cdot S \cdot Q_{\max}}{w}$ is the peak unit stream power, $g = 9.81$ m/s^2 is the acceleration due to gravity, S is the channel slope equal to 0.0011 m/m, $Q_{\max}$ is the maximum discharge within the hydrological period P_i, $w = 77$ m is the median active channel width of the reach, $R_g = \rho_s/\rho - 1$ is the relative density of submerged sediments, and D_{50} is the median grain size.

Tracer studies also found that the measured distributions of travel lengths may be described by an exponential probability distribution (e.g., Hassan & Bradley, 2017; Papangelakis & Hassan, 2016; Phillips & Jerolmack, 2014; Vázquez-Tarrío et al., 2023):

$$P(L) = \lambda \cdot e^{-\lambda \cdot L} \tag{4}$$

where $P(L)$ is the probability of a given tracer travel distance L, and λ is the inverse of $\overline{L}$.

Based on this, we proposed a workflow for modeling tracer dispersion in the Ain River. We applied this workflow to each one of the survey periods (2013–2014, 2013–2015, and 2013–2017) and we compared the field observations with the estimated displacements. Thus, we tried to understand the main reason for tracer loss in our surveys, which could be related to the loss of frontrunners, tracer burial or incomplete prospection of the surveyed area (MacVicar & Papangelakis, 2022). The workflow consisted of the following four steps:

1. We computed the mean travel distance of tracers based on the empirical relations linking mean travel distance to dimensionless stream power (Equation 3), reported by Vázquez-Tarrío et al. (2019). Note that we employed the D_{50} of the tracers (41 mm) to compute the dimensionless stream power for the first hydrological period. We then used the D_{50} of the surface riverbed (80 mm) for the second and third hydrological periods. For the first hydrological year, tracers departed from unconstrained bed conditions, and in the second and third hydrological periods we assumed that tracers were progressively mixed into the bed structure (constrained bed conditions) (see Figure 8 in Vázquez-Tarrío et al., 2019). To fit their regression equation linking travel distances to dimensionless stream power, Vázquez-Tarrío et al. (2019) normalized $\overline{L}$ by a measure of the spacing between macroforms, that is 5.7 times the active channel width in the case of riffle-pool rivers, following Montgomery and Buffington (1997) and Pyrce and Ashmore (2005), who reported how patterns of particle deposition are related to the pool and bar morphology. In the present work, we used the same nondimensionalization for the tracer travel distances, that is, $5.7 \cdot w = 439$ m.
2. We generated a population of 10,000,000 tracer displacements using an exponential distribution function with a mean equal to the mean tracer travel distance estimated in step 1.
3. We take 10,000 samples of n displacements (with $n = 862$, the number of analyzed tracer particles in the Ain River) from the population generated in step 2.
4. We computed the cumulated distribution function of the 10,000 mean travel distances to get a robust approximation of the expected frequency distribution of tracer displacements.

We also compared the tracer travel distances measured in the field with the cumulated distributions of travel distances derived from the 2D hydrodynamic model. In this way, we evaluated whether or not the numerical model can provide reliable characterizations of particle dispersion.

3.3. Numerical Modeling

3.3.1. Development of the 2D Model

A 2D hydrodynamic model of the approximately 40 km-long main channel of the Lower Ain River between Pont d'Ain and the confluence with the Rhône River was constructed. The Barré-de-Saint-Venant equations were solved using the Rubar20 software (Bessenasse et al., 2004; El Kadi Abderrezzak et al., 2009) on a mesh aligned along the flow direction and made of quadrilaterals and triangles with an average cell area of 5.5 m^2 (Figure 4a).

The topography of the floodplain, dry-bed areas, and the in-stream channel was obtained from topo-bathymetric aerial light detection and ranging (LiDAR) survey performed in August 2015 with an average of 18 points/m^2 for a low-flow discharge of 16 m^3/s (Figure 4b). The XYZ accuracy was estimated to be better than 0.08 m for dry areas and better than 0.10 m under water. The total percentage of underwater areas covered by the LiDAR survey is 30%. The point density decreased with water depth and explained the lower accuracy, especially for areas deeper than 2.5 m (maximum depth: 4 m). However, there were only 11% underwater areas deeper than 1 m at 16 m^3/s, and 1% deeper than 2.5 m. The bed friction was calibrated based on water long profiles for the main channel (Strickler coefficient values between 20 and 40) for the two discharges of 90 and 16 m^3/s, corresponding to field (differential GPS) and LiDAR surveys, respectively. For 90 m^3/s, the difference between measured and simulated water surface elevations was smaller than 0.1 m for 90% of the points, and smaller than 0.15 m for 99% of the points. For the floodplain and areas inundated when discharge exceeds 90 m^3/s, the bed friction was estimated based on land use

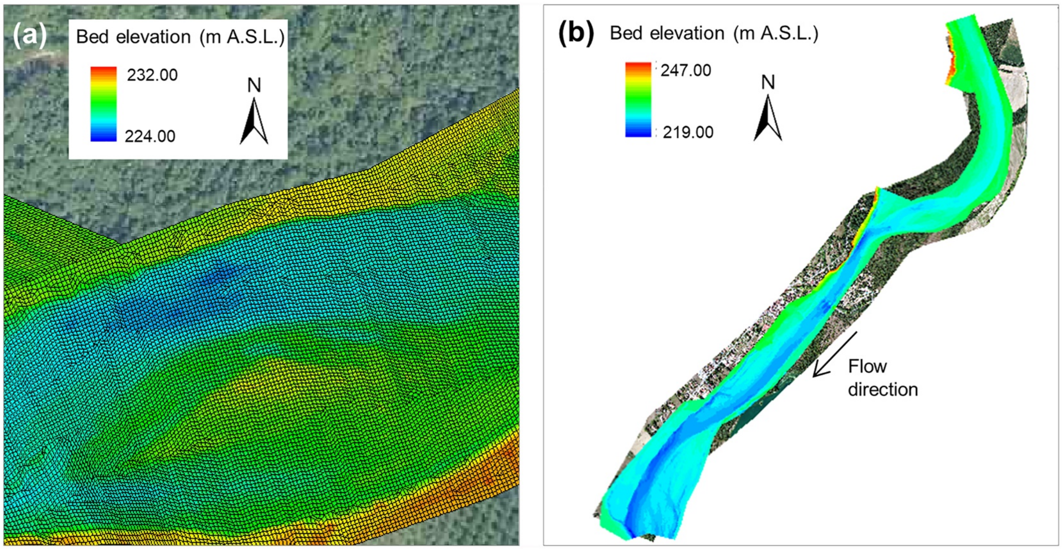

Figure 4. (a) Close-up view of the computational grid upstream from Priay. (b) General view of the 2D numerical model of the Ain River used in the present study.

(Strickler coefficient values between 15 and 40). The simulated flow velocity field agreed well (bias of 0.06 m/s, i.e., 5% of the mean flow velocity of 1.11 m/s, and root mean square error of 0.34 m/s for the velocity intensity) with acoustic Doppler current profiler (ADCP) measurements conducted along 18 cross-sections in December 2013 (flow discharge varying between 116 and 206 m^3/s), excluding data from the vicinity of bridge piers where the flow was highly disturbed and three-dimensional. There was a single relatively large flood event between the ADCP surveys performed in 2013 and the LiDAR survey performed in 2015, but not long enough (8 hr > Q_2 on 30 March 2015) to cause significant changes in channel geometry and thus affect the flow velocity field.

For the present study, only the section of the model between Terre Soldat and Villette-sur-Ain was used. The model was run with the discharge time series at Pont d'Ain averaged over 2 hours to obtain the steady flow patterns at three representative flow discharges of 350, 500, and 760 m^3/s, which correspond to the critical discharge for incipient sediment transport, an intermediate flow discharge, and the 2-year flood discharge. The computational time would have been too long in unsteady flow conditions over the period 2013–2017 (several weeks or even several months), hence the strategy of computing a few representative steady flows only.

3.3.2. Computation of Particle Trajectories

The entire population of recovered tracers was modeled, that is, 321, 473, and 344 particles in the three surveys, respectively. Field-measured and modeled trajectories were compared for each tracer particle based on the tracer IDs.

The trajectory of particles was calculated for each size class based on hydrodynamic modeling results. We used the equation of Engelund and Fredsøe (1976) for the bedload transport velocity u_b:

$$u_b = \begin{cases} 10\,u_*\left(1 - 0.7\sqrt{\tau_c/\tau}\right) & \text{if } \tau > 0.5\tau_c \\ 0 & \text{if } \tau \le 0.5\tau_c \end{cases} \tag{5}$$

Where τ is the bed shear stress calculated from the friction slope J (using $\tau = \rho{\cdot}g{\cdot}H{\cdot}J$), H is the water depth, $u_* = \sqrt{\tau/\rho}$ is the friction velocity, and τ_c is the critical bed shear stress calculated from the mean diameter of a particle size class D_m (Meyer-Peter & Muller, 1948):

$$\tau_c = 0.047 \cdot D_m \cdot (\rho_s - \rho) \cdot g \tag{6}$$

For a given size class (D_m = 25, 34, 48, 72, and 97 mm), the particle velocity was calculated using the discharge time series at Pont d'Ain averaged over 2 hours, assuming that the particle velocity was zero below 350 m^3/s, and varied linearly with the flow from 350 to 500 m^3/s and 500–760 m^3/s.

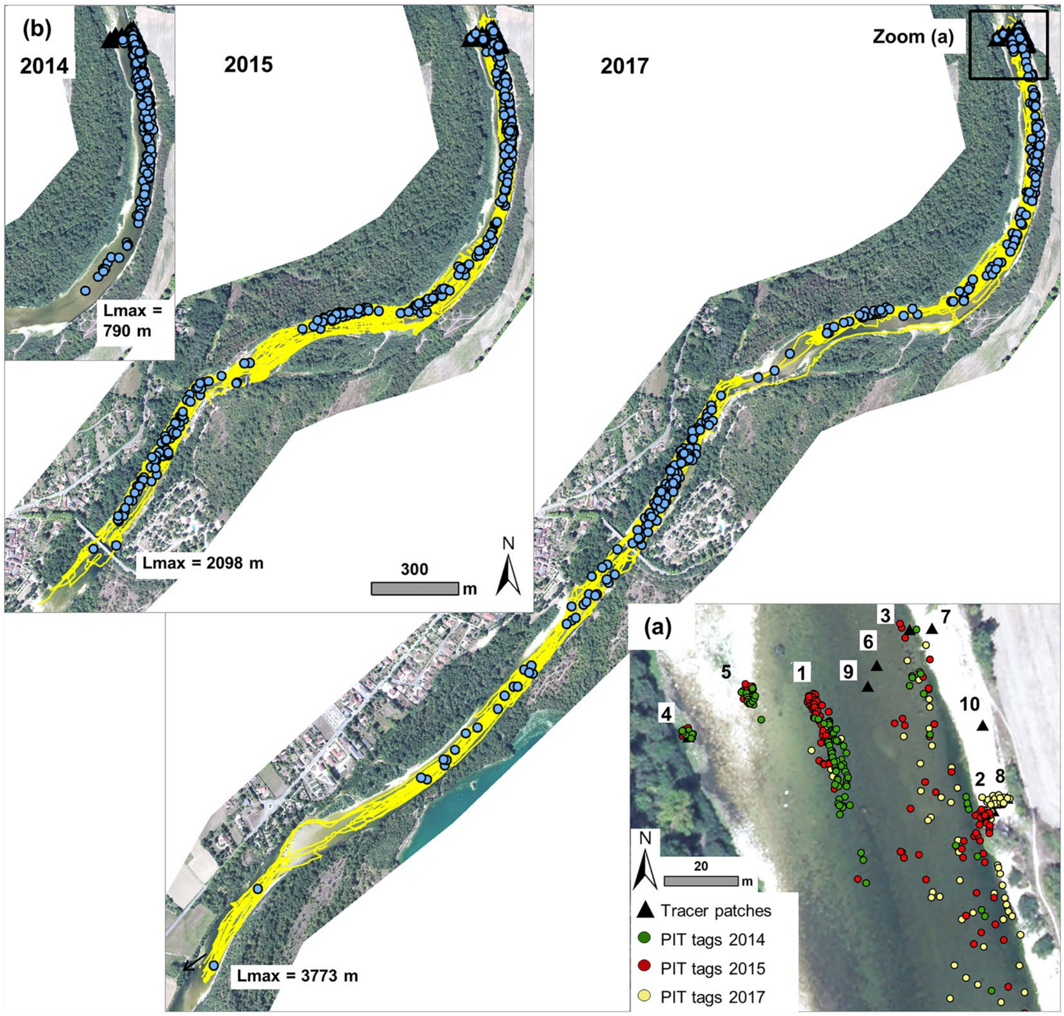

Figure 5. (a) Positions of the 10 tracer patches in 2013 and the detected tracers in 2014, 2015, and 2017. Immobile tracers from patches number 4 and 5 are shown. (b) Position of the tracer cloud and the GPS tracking courses (yellow lines, except for 2014) over time. Base map: ORTHO HR® IGN 2015.

The critical bed shear stress of one individual particle is $\tau_{ci} = \tau_c D_i/D_m$, where D_i is the grain size of the individual particle of a class with a mean diameter D_m, and the critical bed shear stress τ_c and bed shear stress close to the inception of movement are similar ($\tau \approx \tau_c$). The velocity of this individual particle u_{bi} can thus be computed as the class velocity multiplied by the ratio of the class diameter to the individual particle diameter, that is, $u_{bi} \approx u_b\, D_m / D_i$. Therefore, two particles of the same size class but having a different diameter and starting from the same point, can have a slightly different trajectory.

At each calculation time step, the particle velocity can be calculated from the hydrodynamic results at the center of the cell closer to the current particle location. The trajectory of the particle was calculated from the beginning of the period until the end of the period. A time step of 50 s was selected so that a particle cannot travel through more than one neighboring cell within one time step. A smaller time step would have increased the calculation time without increasing the accuracy, considering that the flow discharge was only modified every 2 hours. The bedload transport direction, which was used to compute particle trajectories, was estimated considering that the sediment transport direction may deviate from the flow velocity direction because of the transverse bed slope effect The particle velocity was partitioned into downstream and cross-stream components, each including a deviation angle ψ (Talmon et al., 1995):

$$\tan\psi = -7\frac{H}{R} - \frac{1}{0.85 \cdot \sqrt{\theta}}\frac{\partial Z}{\partial n} \tag{7}$$

where R is the radius of curvature of the streamlines, θ is the non-dimensional shear stress, Z is the channel bed elevation, and n is the normal to the streamlines (the derivative function used is therefore the channel slope perpendicular to the velocity). The values 7 and 0.85 were taken from Engelund (1974) and Mosselman (1998), respectively.

4. Results

4.1. Field Tracer Results

The travel of tracer particles depended on their seeding positions (Figure 5a): tracers seeded on the restored left bank (i.e., patches number 2, 3, 7, 8 and 10) and in the adjacent channel (patches number 6 and 9) were transferred downstream, whereas tracers seeded near the right bank (patches number 4 and 5) remained at their initial positions. Tracers seeded in the middle of the channel (patch number 1) traveled no more than 40 m after 4 years. None of the tracers seeded on the bank top (patches number 7 and 10) were detected at their initial positions, which proved that the artificial sediment supply was rapidly remobilized, except for tracers in patch number 8, on the downstream end of the restored bank, which did not move during the first survey and were then exported downstream. The percentage of mobile tracers is 56%, 71%, and 69% for the 2014, 2015, and 2017 surveys, respectively.

Tracers were increasingly dispersed over time. Between 2014 and 2017, the position of the tracer cloud centroid changed from 145 to 1,054 m, and the standard deviation increased from 179 to 905 m. The travel distance of the tracer cloud centroid (L_T) was 123 m, 458 and 451 m during P_1, P_2 and P_3, respectively. The farthest traveling tracer was found 3,773 m downstream of its seeding site in 2017. The dominant spatial pattern of tracer trajectories during P_1 was a translation from the left bank to the right bank in the river bend (Figure 5b). During P_2, we observed preferential areas for tracer deposition on riffles and preferential longitudinal transport veins up to the Priay bridge and downstream. These preferential areas were fairly consistent with the bed elevation profile (Figure 9b): the section at 1,000–1,200 m in the channel bend is a pool with lower bed shear stresses and many tracers have been found here in 2015. The upstream section of the Priay bridge (1,600–2,000 m) exhibits a convex bed profile and it was a preferential depositional area in 2015 and 2017. For each hydrological period, the mean travel distance of the individual mobile tracers that were recovered in successive surveys ($\overline{L_{sm}}$) was 214 m, 546, and 553 m. The virtual velocity of mobile tracers was 1.37 m/hr, 2.31 m/hr, and 1.53 m/hr.

4.2. Validation of Literature-Based Simulations of Tracer Travel Distances

We compared our field observations for the Ain River with previous data compiled from the literature to better understand the causes of tracer loss during our field surveys, thus improving our interpretation of the observed distribution of tracer travel distances. In Figure 6a, the mean travel distance $\overline{L}$ of particles, normalized by the morphological length scale of the channel, is plotted as a function of the dimensionless stream power ω^*. Our tracer observations for the Ain River were very close to the main trend documented by Vázquez-Tarrío et al. (2019) (residual value of 0.44, −0.66, and −1.17 for the three field surveys). Concerning the cumulated frequency distribution of tracer displacements, the measured distributions for the different tracer surveys in the Ain River tended to collapse into a common trend when individual tracer displacements were normalized by the mean travel distance. This common trend may be described by an exponential probability distribution, as described in Equation 3 (Figure 6b). Normally, the exponential distribution is used to approximate "memoryless" processes, that is, hop distances for an individual tracer are not dependent on the previous hop distances.

Using these findings, we applied the workflow described in Section 3.2 to derive the distribution of tracer travel distances for the Ain River. The estimated and field-measured distributions followed a similar trend, although the field data show a bimodal distribution that is not adequately grasped with the estimated distribution (Figure 7). Indeed, there were some preferential zones for the particles to deposit, leading to a second peak in the distribution at 1,800–2,000 m. Another difference between the estimated and field results relates to the tracers traveling moderate distances (200–1,000 m), which were recovered in the field. The mass excess of tracers between 1,600 and 2400 m in the field data is 72 tracers, while the mass excess of tracers in the exponential model between 200 and 1,000 m is 377 tracers. This implies that most of the tracers may have remained in the surveyed area, buried, affected by signal collision or missing because of insufficient density prospection, rather than being due to pebbles traveling further than the prospected area. If this is the case, then the metrics for particle displacements derived from our field surveys (i.e., mean travel distance, standard deviation) should be reliable and not far from the true values.

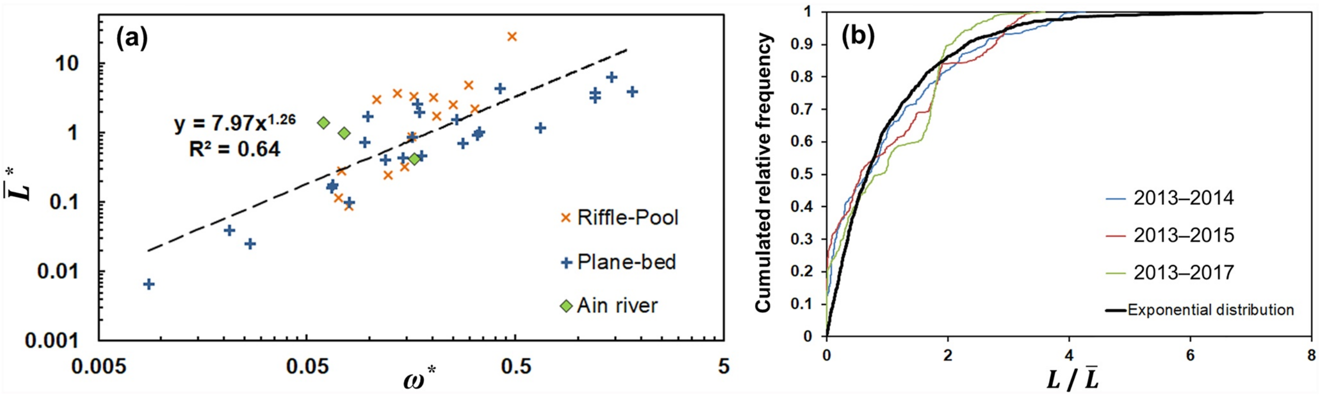

Figure 6. (a) $\overline{L}$ normalized by the morphological length scale of the channel, plotted versus ω^*. Riffle-pool and plane-bed data come from the compilation by Vázquez-Tarrío et al. (2019). (b) Empirical cumulated distributions of $\frac{L}{\overline{L}}$ for the different study periods and theoretical exponential distribution (Equation 3).

4.3. Numerical Modeling of Particle Displacement

The 2D hydrodynamic model provides a map of the bed shear stresses for each flow discharge. Figure 8a shows a magnified view of this map for a discharge equal to 760 m^3/s. A significant spatial variability of the bed shear stress is observed in the river reach, with low bed shear stresses outside the main channel due to low water depth and low-flow velocity and high bed shear stresses at the bifurcation between the main channel and the secondary channel. However, the bed shear stresses remain relatively homogeneous within the channel cross-section, but they vary longitudinally according to the bed elevation profile (Figure 9). The average bed shear stress varies from about 25 Pa at 350 m^3/s to about 35 Pa at 760 m^3/s. As a comparison, the critical bed shear stress for the inception of movement varies from 20 to 76 Pa for grain sizes ranging from 25 to 97 mm. Thus, large particles did not move in the model while small particles moved over relatively long distances (Figure 12). For the lowest modeled discharge (350 m^3/s), even small tagged particles hardly moved, which is consistent with this discharge level being critical for incipient bed movement.

The locations where the modeled tracers and field tracers deposited are generally different (Figures 8b and 8c). The model does not yield as many distributed positions as the field observations, and the model yields preferential deposition in some areas where the computed flow velocity is low. Since the model tends to overestimate the flow entering the left-bank secondary channel in the meandering curve (Figure 8b), it leads to erroneous preferential stopping positions. The downstream end of the secondary channel was prospected in 2015 (see GPS course lines in Figure 5b) and no tracer had been found.

The comparison of the modeled travel distances with the results derived from the probabilistic approach shows that, unlike the probability model, the numerical model can reproduce the bimodal distribution observed during

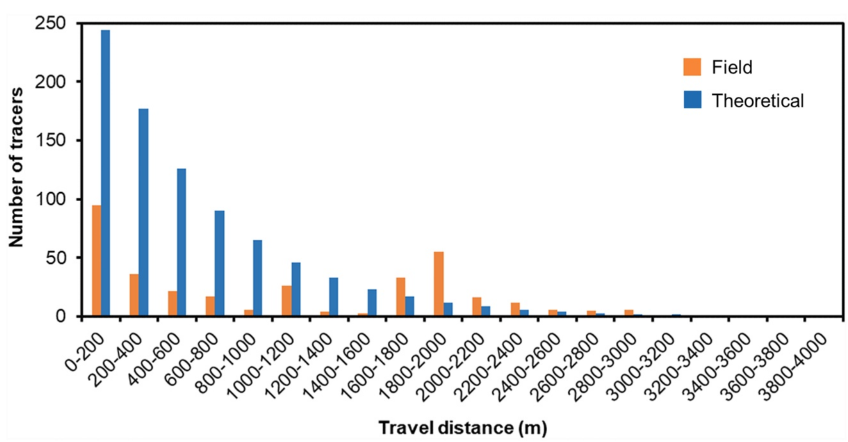

Figure 7. Comparison between the observed distribution of tracer travel distances for the Ain River and the distribution of estimated travel distances based on the workflow described in Section 3.2, for 2013–2017.

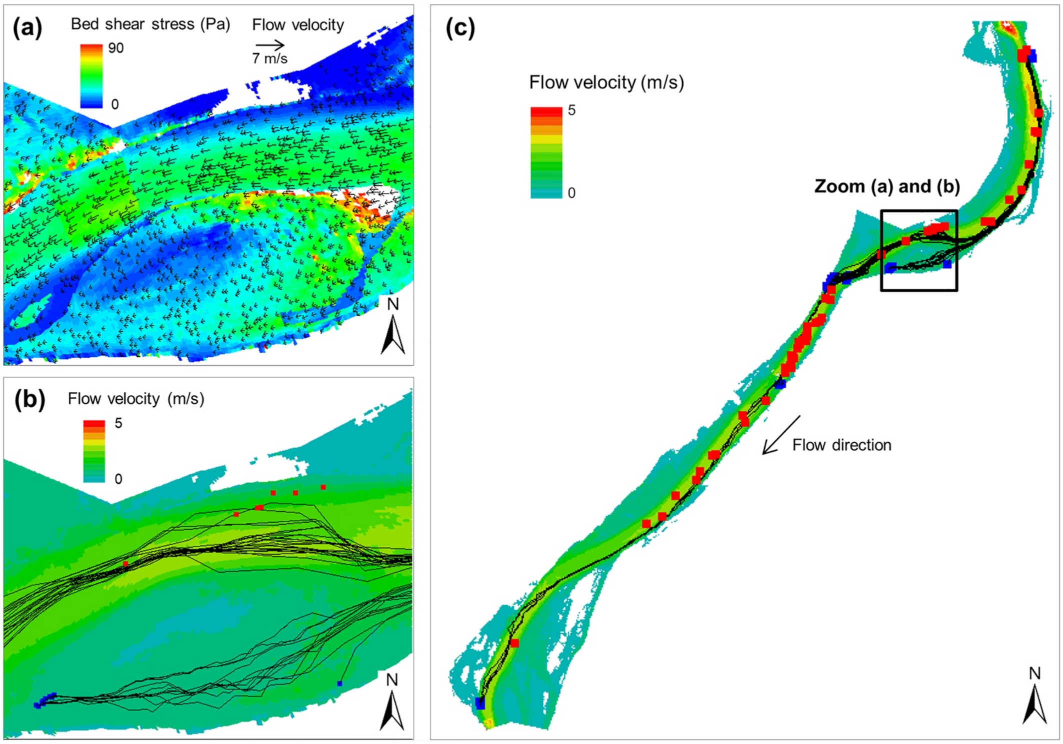

Figure 8. (a) Detailed map of the bed shear stress calculated by the model for the discharge of 760 m^3/s with (b and c for the larger map) flow velocity and modeled trajectories (black lines) of the particles in the grain size class 17–32 mm from 2013 to 2017 (red squares: final field-measured locations; blue squares: final modeled locations).

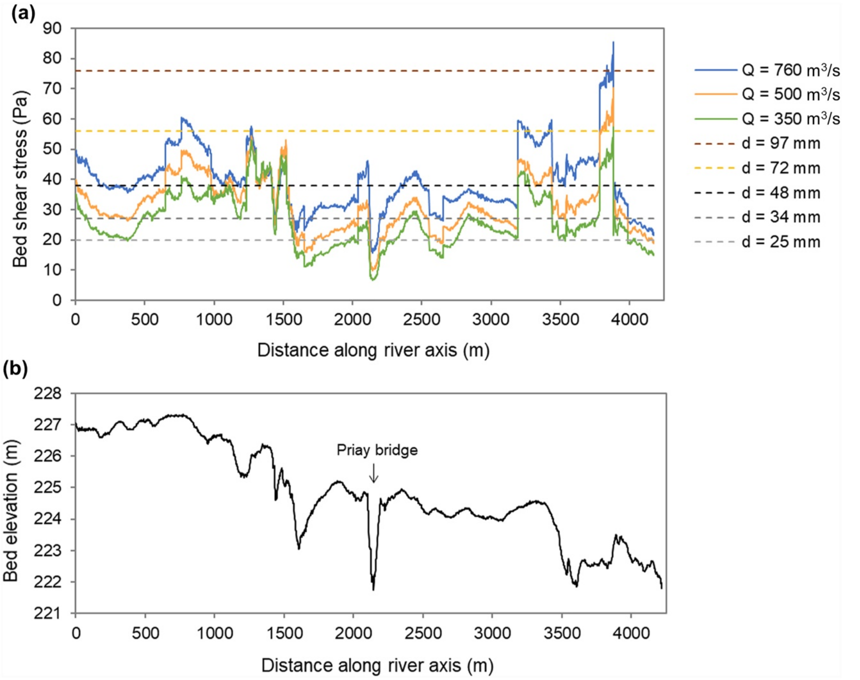

Figure 9. (a) Longitudinal distribution of bed shear stresses along the channel centerline, calculated by the model for discharges of 350, 500, and 760 m^3/s. Dotted lines indicate the critical shear stress for each particle size class. (b) Bed elevation profile along the channel centerline.

the field surveys (Figure 10). The numerical model highlights the non-linearity of the sediment dynamics along the river reach with areas of tracer accumulation, although the deposition places observed in the field are not reproduced exactly. Additionally, the number of tracers that did not move as predicted by the numerical model approaches the observations in the field (Figure 11), suggesting that the inception of movement within the river system is properly modeled, at least for the coarse particles.

Figure 12 compares the modeled and field-measured mean travel distances for the different size classes of the mobile particles. Field observations show an increasing effect of particle size on the travel distances over time. Smaller particles traveled longer distances than larger particles, especially in the second and third hydrological periods after particle seeding. The effect of grain size was not significant during the first displacement after particle seeding. Modeled travel distances are generally overestimated for finer particles, particularly the size classes of 17–32 and 32–45 mm. The effect of grain size on the travel distance appears to be reproduced well by the model in the second and third hydrological periods, although no displacement is modeled for the particles from 90 to 120 mm.

5. Discussion

5.1. Feedback on RFID Particle Tracking

Methodological improvements have been made in the present RFID monitoring study compared with previous studies using PIT tags in medium to large rivers, such as the Ain and the Rhine rivers (Arnaud et al., 2017; Rollet et al., 2008). For instance, mixing 23 and 32 mm-long tags, logging the GPS course line, logging the detected tags that suppressed manual errors and delays and provided very satisfying tracer double analysis, were advantageous capabilities. These improvements significantly increased the number of recovered tracers compared to previous studies in large rivers. Generally, lower recovery rates obtained in large rivers are compensated by the seeding of larger populations of tracers, such as on the Ain River, leading to an absolute number of recovered tracers comparable to that obtained in small rivers (Piégay et al., 2016a).

Particle tracking provides important insights to assess the physical effects of river restoration, especially gravel augmentation. Tracer patches that have been remobilized inform on the thresholds for particle entrainment according to their seeding location and the optimal design for the artificial deposit. In the Ain River, almost all the tracers seeded on the bank have moved downstream from the first hydrological period that included moderate flow events below Q_2. Thus, the RFID tracking study confirmed the efficiency of gravel augmentation on a concave bank like that of Terre Soldat.

Tracer travel distances and trajectories can then help to identify preferential deposition sites and thus channel units that benefit from gravel augmentation. In our study reach, the two depositional and vegetated forms visible on the right bank (see arrows in Figure 1b) correspond to the "B1" site where 10,000 m^3 of sediments were supplied in 2005 (Lejot et al., 2011). This site is located in a less dynamic area with relatively low bed shear stresses and no tracers were found near this bank. Sediment supplied in 2005 did not move downstream and the artificial deposits were vegetated (Figure 1b). Lejot et al. (2011) performed bathymetric monitoring from UAV images. They identified the downstream "B2" site (8,800 m^3 of supplied sediment) as the starting point of the sediment wave propagation. Our particle tracking provides more information because Figure 5b shows that this site is a temporary storage area for sediments, which can eventually travel beyond the downstream riffle.

The tracer cloud that we surveyed between 2013 and 2017 was progressively fragmented (Figures 5 and 10) and was driven by the bed morphology (Figure 9b), similar to a study on the Rhine River (Chardon et al., 2021). Our values of virtual velocity (1.37–2.31 m/hr) were close to those of studies on riffle-pool rivers, notably fitting well with the Hassan et al. (1992) equation that relates the virtual velocity with the excess stream power (see Figure 9b Chardon et al., 2021). Our values were even slightly higher. This may be an effect of bed armoring, that can act as a booster of longitudinal sediment transport because vertical exchange of particles between sedimentary layers is more difficult in armored rivers (Galia et al., 2021). Bed armoring could also explain the lack of size-selective transport during the first displacement after particle seeding (Figure 12), since the median sizes of the tracers (41 mm) and the augmented gravel (22 mm) were much smaller than the median size of the riverbed (80 mm), and particles were not yet imbricated into the bed structure. Bedload tracing studies then report generally a progressive slow-down of tracers over time, related to vertical mixing into the bed structure and downstream change in bedload transport capacity in a concave river profile, the former occurring especially in the context of

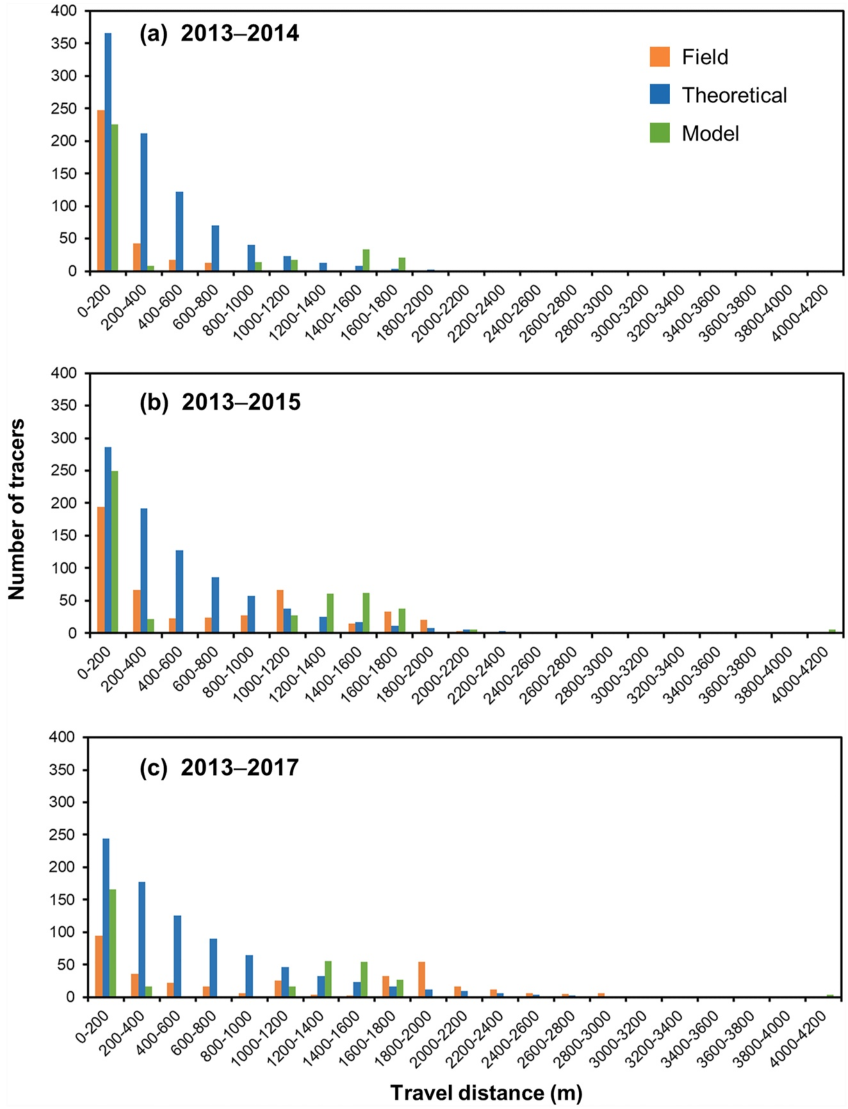

Figure 10. Comparison among the field-measured distribution of tracer travel distances, the estimated distribution based on previous literature, and the distribution derived from the numerical model.

gravel augmentation where the artificial sediment input is often unsorted and uncompacted (Chardon et al., 2021; Vázquez-Tarrío et al., 2023). In the Ain River, the virtual velocity increased between P_1 and P_2, then decreased to P_3. The abnormal value during the first period may confirm that the 2014 survey was partial and that frontrunners were under-estimated, as shown by the probabilistic model (Figure 10a).

Finally, RFID tracers are useful to assess the time needed for the sediment wave to exit the restored reach. It is a critical issue for risk evaluation (flooding risk in adjacent areas, threats to downstream infrastructures) and sustainability of the gravel augmentation (Arnaud et al., 2017; Vázquez-Tarrío et al., 2023). Pebble tracking in the Ain River confirmed the need to periodically supply the river with fine gravel since tracers were transported up to four km downstream in only 4 years. This travel distance is consistent with the mean annual propagation of the sedimentary deficit front of approximately 500 m/yr below the Allement Dam (Rollet et al., 2014).

5.2. Quality Survey Estimate From the Probabilistic Approach

To assess the quality of the field observations, we estimated the expected travel distances based on a probability function. One of the main concerns is related to the search area covered by the survey. The expected mean travel distance was estimated for the different periods using the peak discharge for each period and the empirical

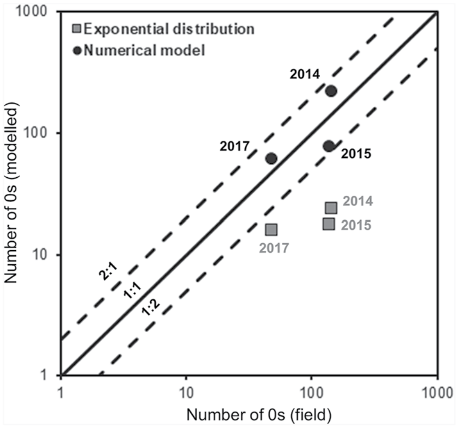

Figure 11. Comparison between the number of immobile tracers (0_s) observed in the field and computed from numerical and probabilistic models.

correlation reported by a systematic review of previous literature on tracer studies (Vázquez-Tarrío et al., 2019). These estimations were then introduced into an exponential frequency distribution function to derive the entire distribution of travel distances expected for the Ain River. Several limitations can be considered in this approach. For instance, the mean travel distances are only based on the peak discharge in each hydrological period, whereas the previous tracer studies suggest that the flow duration also plays a significant role in tracer dispersion (e.g., Hassan & Bradley, 2017; Papangelakis et al., 2022; Phillips et al., 2013). The probabilistic model could be improved by including both peak stream power and flood duration of all events over the transport threshold. However, this would require that the hydrological times series be shared, which is not yet the case for most of reported tracer studies. Moreover, improvement in the calibration of such a probabilistic transport model requires treating different tracer sizes separately, recognizing the sensitivity of the results to threshold estimates and the influence of particle size and channel width on tracer displacements (Beechie, 2001; Church & Hassan, 1992; Papangelakis et al., 2022).

The observed differences in the field and modeled distributions from the probabilistic approach (Figure 10) can be explained by the non-recovered tracers, the uncertainties inherent to field measurements of bedload transport, as well as the longitudinal heterogeneity of the flow, which can help explain preferential zones of deposition, as shown in the numerical model. We believe the probabilistic approach provides a useful way to contextualize our field observations in a wider framework and discuss the reasons for tracer loss. In this regard, our results suggest that non-recovered tracers in 2015 and 2017 relate mostly to the loss of buried tracers or an incomplete prospection of the surveyed area, and not to missing frontrunners. Thus, the metrics for travel distances derived from our field observations are considerably reliable.

5.3. Potential of a 2D Numerical Model for Predicting Particle Displacement

The trajectory calculation of individual particles based on hydrodynamic results from the 2D numerical model provided mean travel distances of the same order as the field measurements, without specific calibration for the three finer classes of sediment. The numerical model did a better job for capturing the bimodal distribution of the tracer cloud, which could not be captured by the exponential model (Figure 10). It also mostly reproduced travel distances by size class (Figure 12).

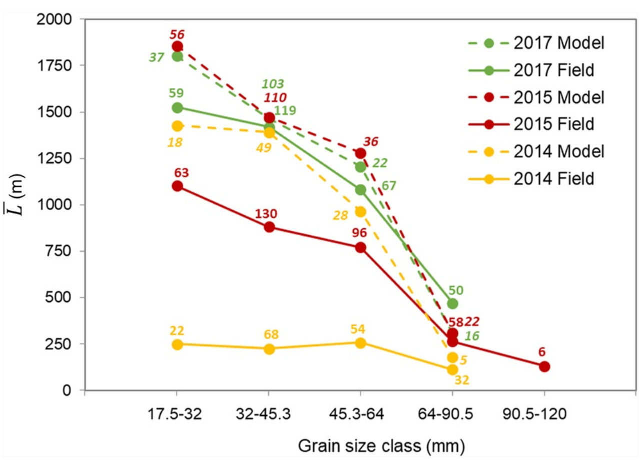

Figure 12. Field-measured and modeled mean travel distance $\overline{L}$ versus particle size. Labels indicate the numbers of tracers in each class for field and modeled data. Samples with less than five particles are not shown. Immobile tracers were excluded.

Since the numerical model for particle trajectory is deterministic, it was expected that some disagreement can be observed for a few specific particles. There is a bias linked to the calculation method for the particle trajectory, such that one particle stops only if the bed shear stress at its location is below the critical bed shear stress; otherwise, it continues traveling downstream. Deposition in the center of the main channel does not occur, and generally, particles only stop at specific locations (e.g., close to the initial location, on particular locations on the banks, or in secondary channels). Two reasons can be argued: the interaction between particles was not modeled (hiding and protrusion effects; Wilcock, 1988), and the modeling of the transport interference is too crude. More generally, as discussed by several authors (Camenen & Larson, 2005; Perret et al., 2023; Recking, 2010), a model based on the excess bed shear stress may not be adequate to simulate such stochastic behavior. When the bed shear stress is below the critical value for a particular size class, no transport can occur (Figure 9). As a consequence, such a model is sensitive to the choice of the critical Shields number (taken here as equal to 0.047), and significant uncertainties exist for this value (Buffington & Montgomery, 1997; Perret et al., 2023).

Some particles were calculated beyond the location of the surveyed frontrunner (maximum calculated travel distance of 4,139 m in 2015 and 2017; Figures 10b and 10c), maybe indicating that the surveyed area was not long enough or that the criteria for depositing particles was not strict enough. Since the field results were confirmed by the probabilistic approach on average, one can assume that the criteria used in the numerical model for starting and stopping particle movement should be revised, considering the environment of the particle and not only the bedload velocity. This is particularly true in straight sections: a particle transported along the channel axis remains there and always has a transport velocity as long as the discharge is sufficient. Hence some particles can travel completely downstream of the model. This could explain why in 2015 and 2017 (Figure 10), the modeled tracer deposition was closed to 1,200–1,800 m whereas for field observations, the deposition occurred at 1,600–2,000 m in the straight section upstream of the Priay bridge, where the bed profile is convex (Figure 9b). By giving a probability of final stopping, some particles could stop in straight sections but the main limit of the model is that particles deposit too easily in channel bends. Increasing the deviation angle by changing the coefficients in Equation 7 would modify the trajectories of individual particles and result in a distribution of deposits better balanced between the left and right banks.

It is also possible to add some equations in the model to account for potential hiding and protrusion effects (Wilcock, 1988). However, as discussed before, the excess bed shear stress as well as the inherent uncertainties in the evaluation of the critical bed shear stress yield larger uncertainties already. We believe that including the role of bed structure (using existing models and available data) would not change significantly the results. Yet, the model, which has not been recalibrated, shows some interesting behavior. To match the observations more closely, a moving probability can be introduced to describe the stochastic behavior of bedload transport. A full Lagrangian model may be more accurate to simulate the particle trajectory (Ballio et al., 2018), and using a probability density function for the particle step length may be useful to incorporate stochasticity (Iwasaki et al., 2017).

Particles enter and stop in the secondary channel in the 2D model although no tracer particles were found there in the field (Figure 8b). This may be explained by the vegetation at the upstream end of the channel that is not accounted for in the model. Thus, the accuracy of the bed roughness can lead to uncertainty, as well as the accuracy of the topography (based on aerial LiDAR) in the vegetated zone. In addition, the decrease of the flow velocity is underestimated and the deviation of the particles in the main flow may be miscalculated because secondary currents are not simulated in such a 2D depth-averaged hydrodynamic model. Secondary currents can however play a significant role in trajectories locally, especially around bars and islands (or banks, bridge piers, other obstacles or anywhere the flow is deviated or non-uniform). This may partly explain why some pathways are poorly simulated, irrespective of the deterministic or probabilistic model used.

More generally, a small change in the parameters of the model can change significantly the trajectory of one particle while it does not change the average behavior if the number of particles is sufficient. Then, running the model with various sets of parameters through a sensitivity analysis would provide a better view of the particle dispersion process.

6. Conclusions

This comparative study regarding a gravel-augmented reach of the Ain River in Eastern France highlights the strengths and weaknesses of three state-of-the-art approaches used for determining river gravel mobility. Due to recent technological improvements, sediment tracking using PIT-tagged gravels provides an increasingly reliable representation of the bedload movement in the field. However, the data can be costly to obtain and limited in spatio-temporal resolution. Additionally, an important issue remains, namely the detection of the frontrunner particles. Derived from previous PIT-tag studies, the probabilistic approach based on an exponential distribution and peak discharge over the surveyed period correctly reproduces the average trend in distances traveled by the different classes of particles. This approach provides useful values that enable the discussion of the frontrunners and how to trace them. However, it fails to predict the exact shape of the observed distribution of distances in the field, which reflects local particle trapping linked to the variability of local hydrodynamic conditions. The 2D numerical approach accounts for this variability and can simulate realistic displacement distributions for the different classes of particles with high spatio-temporal resolution. However, the dispersion of the tracer cloud is not well reproduced by the purely deterministic transport model. Improvements to the model can be made regarding the prediction of particle inception of movement, and the introduction of a probability density function may produce more accurate results that can describe the stochastic behavior of gravel transport.

In conclusion, the first two approaches presented in this study—PIT-tag surveys and probabilistic modeling—are now relatively well established in the gravel mobility literature, and their combination allows for enhanced robustness and quality of tracer displacement surveys. The third approach based on numerical modeling is an emerging approach, which makes our paper original because it is the first time that the estimation of mean travel distances, the application of an exponential distribution, and the comparison with a hydrodynamic model have been combined. Our results demonstrate that it is more effective to combine a 2D numerical model and a probabilistic model.

Conflict of Interest

The authors declare no conflicts of interest relevant to this study.

Data Availability Statement

Data sets for this research are freely available under the terms of the Creative Commons Attribution 4.0 International (CC BY) license in the PANGAEA data repository (Arnaud et al., 2023). The Rubar20 software is open-source (BSD 3 license) and the code is freely available at: https://gitlab.irstea.fr/theophile.terraz/rubar20. Information is also available at: https://riverhydraulics.inrae.fr/en/tools/numerical-modelling/2d-modelling-rubar20-and-rubar20ts/.

Acknowledgments
The research was funded by the LTSER Zone Atelier Bassin du Rhône, Électricité de France (EDF), and the Rhône-Méditerranée-Corse Water Agency (Action B15). The numerical modeling was funded additionally by the EcoFlowS research team in INRAE. The work was performed within the framework of the EUR H2O'Lyon (ANR-17-EURE-0018) of the Université de Lyon through the "Investissements d'Avenir" program operated by the French National Research Agency. We thank the Lower Ain River syndicate (SR3A) for information on river restoration measures. We are grateful to A. Barillier (EDF-CIH) who provided topo-bathymetric LiDAR data processed by D. Lague (University Rennes 1). We thank colleagues who helped with fieldwork and numerical modeling: H. Capra, S. Monnet, L. Bultingaire, M. Cassel, C. Mouquet-Noppe, T. Dépret, J. Guérin, and R. Jenkinson. Finally we thank Andrea Castelletti, an associate editor and three external reviewers for their fruitful comments and suggestions on the manuscript.

References

Amoudry, L. O., & Souza, A. J. (2011). Deterministic coastal morphological and sediment transport modeling: A review and discussion. *Reviews of Geophysics*, *49*(2), RG2002. https://doi.org/10.1029/2010RG000341

Arnaud, F., Paquier, A., Vázquez-Tarrío, D., Camenen, B., Le Coz, J., Michel, K., et al. (2023). Field, probabilistic and 2D numerical modeling dataset on gravel mobility in the Ain River (2013–2017) [Dataset]. PANGAEA. https://doi.org/10.1594/PANGAEA.954231

Arnaud, F., Piégay, H., Béal, D., Collery, P., Vaudor, L., & Rollet, A. J. (2017). Monitoring gravel augmentation in a large regulated river and implications for process-based restoration. *Earth Surface Processes and Landforms*, *42*(13), 2147–2166. https://doi.org/10.1002/esp.4161

Arnaud, F., Piégay, H., Vaudor, L., Fantino, G., & Bultingaire, L. (2015). Technical specifications of low-frequency radio identification bedload tracking from field experiments: Differences in antennas, tags and operators. *Geomorphology*, *238*, 37–46. https://doi.org/10.1016/j.geomorph.2015.02.029

Ballio, F., Pokrajac, D., Radice, A., & Hosseini Sadabadi, S. A. (2018). Lagrangian and Eulerian description of bed load transport. *Journal of Geophysical Research: Earth Surface*, *123*(2), 384–408. https://doi.org/10.1002/2016JF004087

Beechie, T. J. (2001). Empirical predictors of annual bed load travel distance, and implications for salmonid habitat restoration and protection. *Earth Surface Processes and Landforms*, *26*(9), 1025–1034. https://doi.org/10.1002/esp.251

Bessenasse, M., Kettab, A., & Paquier, A. (2004). Modélisation bidimensionnelle du dépôt de sédiments dans un barrage en Algérie [Two–dimensional modeling of sediments deposits in dam reservoirs in Algeria]. *La Houille Blanche*, *1*, 31–36. (in French). https://doi.org/10.1051/lhb:200401003

Biron, P. M., Carver, R. B., & Carré, D. M. (2012). Sediment transport and flow dynamics around a restored pool in a fish habitat rehabilitation project: Field and 3D numerical modelling experiments. *River Research and Applications*, *28*(7), 926–939. https://doi.org/10.1002/rra.1488

Bradley, D. N. (2017). Direct observation of heavy-tailed storage times of bed load tracer particles causing anomalous superdiffusion. *Geophysical Research Letters*, *44*(24), 12227–12235. https://doi.org/10.1002/2017GL075045

Bradley, D. N., & Tucker, G. E. (2012). Measuring gravel transport and dispersion in a mountain river using passive radio tracers. *Earth Surface Processes and Landforms*, *37*(10), 1034–1045. https://doi.org/10.1002/esp.3223

Buffington, J. M., & Montgomery, D. R. (1997). A systematic analysis of eight decades of incipient motion studies, with special reference to gravel-bedded rivers. *Water Resources Research*, *33*(8), 1993–2029. https://doi.org/10.1029/96WR03190

Camenen, B., & Larson, M. (2005). A general formula for non-cohesive bed load sediment transport. *Estuarine, Coastal and Shelf Science*, *63*(1–2), 249–260. https://doi.org/10.1016/j.ecss.2004.10.019

Camenen, B., Le Coz, J., Paquier, A., & Lagouy, M. (2010). An estimation of gravel mobility over an alpine river gravel bar (Arc en Maurienne, France) using PIT-tag tracers. In *Paper presented at river flow 2010 international conference, Braunschweig, Germany*.

Cassel, M., Piégay, H., Fantino, G., Lejot, J., Bultingaire, L., Michel, K., & Perret, F. (2020). Comparison of ground-based and UAV a-UHF artificial tracer mobility monitoring methods on a braided river. *Earth Surface Processes and Landforms*, *45*(5), 1123–1140. https://doi.org/10.1002/esp.4777

Chapuis, M., Bright, C., Hufnagel, J., & MacVicar, B. (2014). Detection ranges and uncertainty of passive Radio Frequency Identification (RFID) transponders for sediment tracking in gravel rivers and coastal environments. *Earth Surface Processes and Landforms*, *39*(15), 2109–2120. https://doi.org/10.1002/esp.3620

Chapuis, M., Dufour, S., Provansal, M., Couvert, B., & de Linares, M. (2015). Coupling channel evolution monitoring and RFID tracking in a large, wandering, gravel-bed river: Insights into sediment routing on geomorphic continuity through a riffle–pool sequence. *Geomorphology*, *231*, 258–269. https://doi.org/10.1016/j.geomorph.2014.12.013

Chardon, V., Schmitt, L., Arnaud, F., Piégay, H., & Clutier, A. (2021). Efficiency and sustainability of gravel augmentation to restore large regulated rivers: Insights from three experiments on the Rhine River (France/Germany). *Geomorphology*, *380*, 107639. https://doi.org/10.1016/j.geomorph.2021.107639

Church, M., & Hassan, M. A. (1992). Size and distance of travel of unconstrained clasts on a streambed. *Water Resources Research*, *28*(1), 299–303. https://doi.org/10.1029/91WR02523

Clark, M. J., Bennett, G. L., Ryan-Burkett, S. E., Sear, D. A., & Franco, A. M. A. (2022). Untangling the controls on bedload transport in a wood-loaded river with RFID tracers and linear mixed modelling. *Earth Surface Processes and Landforms*, *47*(9), 1–16. https://doi.org/10.1002/esp.5376

Eaton, B. C., & Church, M. (2011). A rational sediment transport scaling relation based on dimensionless stream power. *Earth Surface Processes and Landforms*, *36*(7), 901–910. https://doi.org/10.1002/esp.2120

El Kadi Abderrezzak, K., Die Moran, A., Tassi, P., Ata, R., & Hervouet, J. M. (2016). Modelling river bank erosion using a 2D depth-averaged numerical model of flow and non-cohesive, non-uniform sediment transport. *Advances in Water Resources*, *93*(A), 75–88. https://doi.org/10.1016/j.advwatres.2015.11.004

El Kadi Abderrezzak, K., Paquier, A., & Mignot, E. (2009). Modelling flash flood propagation in urban areas using a two-dimensional numerical model. *Natural Hazards*, *50*(3), 433–460. https://doi.org/10.1007/s11069-008-9300-0

Engelund, F. (1974). Flow and bed topography in channel bends. *Journal of the Hydraulics Division*, *100*(11), 1631–1648. https://doi.org/10.1061/JYCEAJ.0004109

Engelund, F., & Fredsøe, J. (1976). A sediment transport model for straight alluvial channels. *Nordic Hydrology*, *7*(5), 293–306. https://doi.org/10.2166/nh.1976.0019

Gaeuman, D. (2014). High-flow gravel injection for constructing designed in-channel features. *River Research and Applications*, *30*(6), 685–706. https://doi.org/10.1002/rra.2662

Galia, T., Škarpich, V., & Ruman, S. (2021). Impact of check dam series on coarse sediment connectivity. *Geomorphology*, *377*, 107595. https://doi.org/10.1016/j.geomorph.2021.107595

Grabowski, R. C., Surian, N., & Gurnell, A. M. (2014). Characterizing geomorphological change to support sustainable river restoration and management. *WIREs Water*, *1*(5), 483–512. https://doi.org/10.1002/wat2.1037

Haschenburger, J. K. (2013). Tracing river gravels: Insights into dispersion from a long-term field experiment. *Geomorphology*, *200*, 121–131. https://doi.org/10.1016/j.geomorph.2013.03.033

Hassan, M. A., & Bradley, D. N. (2017). Geomorphic controls on tracer particle dispersion in gravel-bed Rivers. In D. Tsutsumi & J. B. Laronne (Eds.), *Gravel-bed rivers: Processes and disasters* (pp. 159–184). John Wiley & Sons, Ltd. https://doi.org/10.1002/9781118971437.ch6

Hassan, M. A., Church, M., & Ashworth, P. J. (1992). Virtual rate and mean distance of travel of individual clasts in gravel-bed channels. *Earth Surface Processes and Landforms*, *17*(6), 617–627. https://doi.org/10.1002/esp.3290170607

Iwasaki, T., Nelson, N., Shimizu, Y., & Parker, G. (2017). Numerical simulation of large-scale bed load particle tracer advection-dispersion in rivers with free bars. *Journal of Geophysical Research: Earth Surface*, *122*(4), 847–874. https://doi.org/10.1002/2016JF003951

Juez, C., Battisacco, E., Schleiss, A. J., & Franca, M. J. (2016). Assessment of the performance of numerical modeling in reproducing a replenishment of sediments in a water-worked channel. *Advances in Water Resources*, *92*, 10–22. https://doi.org/10.1016/j.advwatres.2016.03.010

Keller, E. A. (1970). Bed-load movement experiments: Dry creek, California. *Journal of Sedimentary Research*, *40*(4), 1339–1344. https://doi.org/10.1306/74D7219E-2B21-11D7-8648000102C1865D

Kondolf, G. M., Gao, Y., Annandale, G. W., Morris, G. L., Jiang, E., Zhang, J., et al. (2014). Sustainable sediment management in reservoirs and regulated rivers: Experiences from five continents. *Earth's Future*, *2*(5), 256–280. https://doi.org/10.1002/2013EF000184

Lamarre, H., Mac Vicar, B., & Roy, A. G. (2005). Using passive integrated transponder (PIT) tags to investigate sediment transport in gravel-bed Rivers. *Journal of Sedimentary Research*, *75*(4), 736–741. https://doi.org/10.2110/jsr.2005.059

Laronne, J. B., & Carson, M. A. (1976). Interrelationships between bed morphology and bed-material transport for a small, gravel-bed channel. *Sedimentology*, *23*(1), 67–85. https://doi.org/10.1111/j.1365-3091.1976.tb00039.x

Lejot, J., Piégay, H., Hunter, P. D., Moulin, B., & Gagnage, M. (2011). Utilisation de la télédétection pour la caractérisation des corridors fluviaux: exemples d'applications et enjeux actuels [Characterisation of alluvial plains by remote sensing: Cases studies and current stakes]. *Géomorphologie: Relief, Processus, Environnement*, *2*, 157–172. (in French). https://doi.org/10.4000/geomorphologie.9362

Liébault, F., Bellot, H., Chapuis, M., Klotz, S., & Deschâtres, M. (2012). Bedload tracing in a high-sediment-load mountain stream. *Earth Surface Processes and Landforms*, *37*(4), 385–399. https://doi.org/10.1002/esp.2245

Liedermann, M., Tritthart, M., & Habersack, H. (2013). Particle path characteristics at the large gravel-bed river Danube: Results from a tracer study and numerical modelling. *Earth Surface Processes and Landforms*, *38*(5), 512–522. https://doi.org/10.1002/esp.3338

MacVicar, B. J., & Papangelakis, E. (2022). Lost and found: Maximizing the information from a series of bedload tracer surveys. *Earth Surface Processes and Landforms*, *47*(2), 399–408. https://doi.org/10.1002/esp.5255

Marston, R. A., Girel, J., Pautou, G., Piégay, H., Bravard, J. P., & Arneson, C. (1995). Channel metamorphosis, floodplain disturbance, and vegetation development: Ain River, France. *Geomorphology*, *13*(1–4), 121–131. issn: 0169-555X. https://doi.org/10.1016/0169-555x(95)00066-e

Meyer-Peter, E., & Muller, R. (1948). Formulas for bed load transport. In *Paper presented at 2nd meeting of the international association for hydraulic structures research, Delft, The Netherlands*.

Milan, D. J. (2013). Sediment routing hypothesis for pool-riffle maintenance. *Earth Surface Processes and Landforms*, *38*(14), 1623–1641. https://doi.org/10.1002/esp.3395

Montgomery, D. R., & Buffington, J. M. (1997). Channel-reach morphology in mountain drainage basins. *Geological Society of America Bulletin*, *16*. https://doi.org/10.1130/0016-7606(1997)1092.3.CO;2

Mosselman, E. (1998). Morphological modelling of rivers with erodible banks. *Hydrological Processes*, *12*(8), 1357–1370. https://doi.org/10.1002/(sici)1099-1085(19980630)12:8<1357::aid-hyp619>3.0.co;2-7

Muhar, S., Arnaud, F., Aschwanden, H., Binder, W., Broggi, M., Greimel, F., et al. (2019). Chapter 6.2. Restoration: New life for alpine rivers. In A. Muhar, D. Siegrist, G. Egger, & S. Muhar (Eds.), *Rivers of the alps: Diversity in nature and culture*. Haupt Verlag. ISBN: 978-3-258-08117-5.

Papangelakis, E., & Hassan, M. A. (2016). The role of channel morphology on the mobility and dispersion of bed sediment in a small gravel-bed stream. *Earth Surface Processes and Landforms*, *41*(15), 2191–2206. https://doi.org/10.1002/esp.3980

Papangelakis, E., MacVicar, B. J., Montakhab, A. F., & Ashmore, P. (2022). Flow strength and bedload sediment travel distance in gravel bed rivers. *Water Resources Research*, *58*(7), e2022WR032296. https://doi.org/10.1029/2022WR032296

Perret, E., Camenen, B., Berni, C., El Kadi Abderrezzak, K., & Renard, B. (2023). Inception motion of cohesionless particles: An evaluation of the critical bed shear stress and its uncertainty. *Journal of Hydraulic Engineering*, *149*(4), 1–14. https://doi.org/10.1061/JHEND8.HYENG-13101

Phillips, C. B., & Jerolmack, D. J. (2014). Dynamics and mechanics of bed-load tracer particles. *Earth Surface Dynamics*, *2*(2), 513–530. https://doi.org/10.5194/esurf-2-513-2014

Phillips, C. B., Martin, R. L., & Jerolmack, D. J. (2013). Impulse framework for unsteady flows reveals superdiffusive bed load transport. *Geophysical Research Letters*, *40*(7), 1328–1333. https://doi.org/10.1002/grl.50323

Piégay, H., Arnaud, F., Cassel, M., Dépret, T., Alber, A., Michel, K., et al. (2016a). Suivi par RFID de la mobilité des galets: Retour sur 10 ans d'expérience en grandes rivières. *Bulletin de la Société Géographique de Liège*, *67*(2016/2), 77–91. https://doi.org/10.25518/0770-7576.4476

Piégay, H., Kondolf, M. G., & Sear, D. A. (2016b). Integrating geomorphological tools to address practical problems in river management and restoration. In M. G. Kondolf & H. Piégay (Eds.), *Tools in fluvial geomorphology* (pp. 509–532). John Wiley & Sons, Ltd. https://doi.org/10.1002/9781118648551.ch22

Pyrce, R. S., & Ashmore, P. E. (2005). Bedload path length and point bar development in gravel-bed river models. *Sedimentology*, *52*(4), 839–857. https://doi.org/10.1111/j.1365-3091.2005.00714.x

Recking, A. (2010). A comparison between flume and field bedload transport data and consequences for surface based bedload transport prediction. *Water Resources Research*, *46*(3), 1–16. https://doi.org/10.1029/2009WR008007

Roberts, M. O., Renshaw, C. E., Magilligan, F. J., & Brian Dade, W. (2020). Field measurement of the probability of coarse-grained sediment entrainment in natural rivers. *Journal of Hydraulic Engineering*, *146*(4). https://doi.org/10.1061/(ASCE)HY.1943-7900.0001694

Rollet, A. J. (2007). Etude et gestion de la dynamique sédimentaire d'un tronçon fluvial à l'aval d'un barrage: le cas de la Basse Vallée de l'Ain [Analysis and management of the sedimentary dynamic of a fluvial reach downstream a dam: The case of the Ain River]. PhD Thesis. University of Lyon 3. (in French).

Rollet, A. J., MacVicar, B., Piégay, H., & Roy, A. (2008). L'utilisation de transpondeurs passifs pour l'estimation du transport sédimentaire: Premiers retours d'expérience [A comparative study on the use of passive integrated transponders to estimate sediment transport: First results]. *La Houille Blanche*, *4*, 110–116. (in French). https://doi.org/10.1051/lhb:2008047

Rollet, A. J., Piégay, H., Dufour, S., Bornette, G., & Persat, H. (2014). Assessment of consequences of sediment deficit on a gravel river bed downstream of dams in restoration perspectives: Application of a multicriteria, hierarchical and spatially explicit diagnosis. *River Research and Applications*, *30*(8), 939–953. https://doi.org/10.1002/rra.2689

Schneider, J., Hegglin, R., Meier, S., Turowski, J. M., Nitsche, M., & Rickenmann, D. (2010). Studying sediment transport in mountain rivers by mobile and stationary RFID antennas. In *Paper presented at river flow 2010 international conference, Braunschweig, Germany*.

Stähly, S., Franca, M. J., Robinson, C. T., & Schleiss, A. J. (2020). Erosion, transport and deposition of a sediment replenishment under flood conditions. *Earth Surface Processes and Landforms*, *45*(13), 3354–3367. https://doi.org/10.1002/esp.4970

Talmon, A., Van Mierlo, M., & Struikema, N. (1995). Laboratory measurements of the direction of sediment transport on transverse alluvial bed slopes. *Journal of Hydraulic Research*, *33*(4), 495–517. https://doi.org/10.1080/00221689509498657

Vázquez-Tarrío, D., & Batalla, R. J. (2019). Assessing controls on the displacement of tracers in gravel-bed Rivers. *Water*, *11*(8), 1598. https://doi.org/10.3390/w11081598

Vázquez-Tarrío, D., Peeters, A., Cassel, M., & Piégay, H. (2023). Modelling coarse-sediment propagation following gravel augmentation: The case of the Rhône River at Péage-de-Roussillon (France). *Geomorphology*, *428*, 108639. https://doi.org/10.1016/j.geomorph.2023.108639

Vázquez-Tarrío, D., Recking, A., Liébault, F., Tal, M., & Menéndez-Duarte, R. (2019). Particle transport in gravel-bed rivers: Revisiting passive tracer data. *Earth Surface Processes and Landforms*, *44*(1), 112–128. https://doi.org/10.1002/esp.4484

Vericat, D., Wheaton, J. M., & Brasington, J. (2017). Revisiting the morphological approach: Opportunities and challenges with repeat high-resolution topography. In D. Tsutsumi & J. B. Laronne (Eds.), *Gravel-bed rivers: Processes and disasters* (pp. 121–157). John Wiley & Sons, Ltd. https://doi.org/10.1002/9781118971437.ch5

Wilcock, P. R. (1988). Methods for estimating the critical shear stress of individual fractions in mixed-size sediment. *Water Resources Research*, *24*(7), 1127–1135. https://doi.org/10.1029/wr024i007p01127

Williams, R. D., Brasington, J., & Hicks, D. M. (2016). Numerical modelling of braided river morphodynamics: Review and future challenges. *Geography Compass*, *10*(3), 102–127. https://doi.org/10.1111/gec3.12260